PERGAMON

Chemical Engineering Science 54 (1999) 171–183

Chemical Engineering Science

Rise velocity of a swarm of large gas bubbles in liquids

R. Krishna*, M.I. Urseanu, J.M. van Baten, J. Ellenberger

Department of Chemical Engineering, University of Amsterdam, Nieuwe Achtergracht 166, 1018 WV Amsterdam, Netherlands

Received 19 January 1998; accepted 2 September 1998

Abstract

This paper develops a procedure for estimation of the rise velocity of a swarm of large gas bubbles in a bubble column operating in the churn-turbulent flow regime. The large bubble swarm velocity is estimated by introducing two correction factors into the classical Davies–Taylor (1950) relation for rise of a single spherical cap bubble in a liquid

$$V_b = 0.71\sqrt{gd_b}(\mathrm{SF})(\mathrm{AF}).$$

The scale correction factor (SF) accounts for the influence of the column diameter. This correction is given by the Collins relation (*J. Fluid Mech.*, *28*, 97–112, 1967) and is a function of the ratio of the bubble diameter d_b to the column diameter D_T. Volume-of-fluid simulations confirm the validity of the Davies–Taylor–Collins relations for a variety of liquid properties. The acceleration factor (AF) accounts for the increase in the rise velocity of a bubble because of its interaction with the wake of a bubble preceding it. By analysis of video recordings of the interactions between two bubbles, both in-line and off-line, it is found that the acceleration factor AF increases linearly as the vertical distance of separation between the two bubbles decreases. Increasing liquid viscosity reduces this wake acceleration effect. With the aid of an extensive data set on the large bubble swarm velocity in columns of 0.051, 0.1, 0.174, 0.19, 0.38 and 0.63 m in diameter a correlation is developed for the acceleration factor. The large bubble swarm velocity is found to be three to six times higher than that of a single isolated bubble.

Keywords: Bubble columns; Large bubbles; Churn-turbulent flow regime; Bubble rise velocity; Wall effect; Wake acceleration effects; Column diameter influence; Volume-of-fluid simulations

1. Introduction

Bubble column reactors are often operated in the heterogeneous flow regime at high gas throughputs (typically higher than 0.1 m/s), high pressures (gas densities approaching 20 kg/m^3), and in columns of large diameters (approaching 6 m). A simplified picture of the hydrodynamics in the churn-turbulent regime is portrayed in Fig. 1, which shows that the bubble swarm consists of both 'small' and 'large' bubbles. The small bubbles are in the size range of 3 to 6 mm and are either spherical or ellipsoidal in shape depending the physical properties of the liquid (Clift et al., 1978). The large bubbles are typically in the range of 20–80 mm range (De Swart et al., 1996) and these bubbles undergo frequent coalescence and breakup. The large bubbles can have rise velocities approaching 2 m/s (Krishna and Ellenberger, 1996; Wezorke, 1986) and because of the severe bypassing effect, these bubbles largely determine the gas phase conversion. It is therefore important to be able to predict the large bubble velocity. While the estimation of the rise velocity of a swarm of small bubbles is reasonably well established (Clift et al., 1978; Fan and Tsuchiya, 1990), the estimation of the large bubble rise velocity is much more uncertain.

There are two empirical correlations for estimating the rise velocity of swarms of large bubbles. The first one due to Wilkinson et al. (1992) is

$$\frac{V_b\mu_L}{\sigma} = 2.25\left(\frac{\sigma^3\rho_L}{g\mu_L^4}\right)^{-0.273}\left(\frac{\rho_L}{\rho_G}\right)^{0.03} + 2.4\left(\frac{(U-U_{\mathrm{trans}})\,\mu_L}{\sigma}\right)^{0.757}\left(\frac{\sigma^3\rho_L}{g\mu_L^4}\right)^{-0.077}\left(\frac{\rho_L}{\rho_G}\right)^{0.077} \quad (1)$$

*Corresponding author. Tel.: +31 20 527 7007; fax: +31 20 5255604; e-mail: krishna@chemeng.chem.uva.nl.

0009-2509/99/$ – see front matter
PII: S0009-2509(98)00245-0

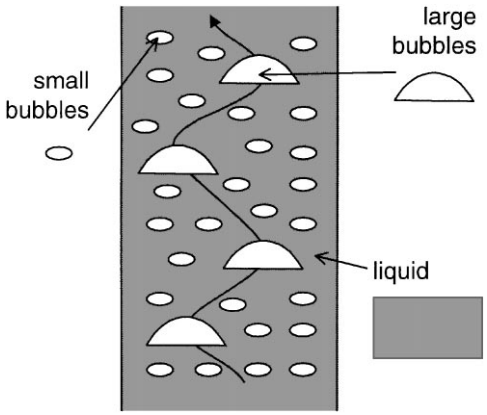

Fig. 1. Picture of churn-turbulent operation of bubble columns.

where U_{trans} is the superficial gas velocity at the point of transition from homogeneous to heterogeneous flow regime. The superficial gas velocity through the large bubble phase is $(U - U_{\text{trans}})$. It is important to note that the Wilkinson correlation does not anticipate that the large bubble rise velocity is column diameter dependent. In a more recent paper, Krishna and Ellenberger (1996) used an extensive set of experimental data obtained in columns of 0.1, 0.174, 0.19, 0.38 and 0.63 m in diameter and with liquids of varying physical properties. They found that the large bubble rise velocity is virtually independent of the properties of the liquid phase but increases significantly with increasing column diameter. They developed the correlation

$$V_b \equiv (U - U_{\text{trans}})/\varepsilon_b = D_T^{0.18}(U - U_{\text{trans}})^{0.42}/0.268\,. \quad (2)$$

Krishna and Ellenberger recommend the use of the Reilly et al. (1994) correlation for the estimation of U_{trans}. An important disadvantage of the Krishna–Ellenberger correlation (2) is that extrapolation to commercial scale reactors is fraught with danger because of the power-law dependence of the large bubble rise velocity on the column diameter. Krishna et al. (1996) suggest the use of eq. (2) up to diameters of 1 m and assert, using analogy with gas–solid fluid beds, that the column diameter dependence ceases after this point. A further point of criticism of both correlations (1) and (2) above is that these cannot be incorporated into more fundamentally based bubble column reactor models using Computational Fluid Dynamics (CFD). Such CFD models, within the Eulerian framework require information on the large bubble sizes and on the interface momentum exchange, or drag, coefficients. (see e.g. Jakobsen et al., 1997).

A careful examination of the literature on CFD modelling of bubble columns (Boisson and Malin, 1996; Delnoij et al., 1997a, b; Devanathan et al., 1995; Grevskott et al., 1996; Grienberger and Hofmann, 1992; Jakobsen, 1993; Jakobsen et al., 1997; Kumar et al., 1995; Lapin and Lübbert, 1994; Lin et al., 1996; Ranade, 1992; Sokolichin et al, 1994, 1997; Torvik and Svendsen, 1990) shows that the simulation of the churn-turbulent regime of operation has not yet been carried out with any degree of success. This failure is in no small measure due to the lack of reliable procedures for estimating the large bubble sizes and the corresponding drag coefficients. The development of this information for use in CFD models is the major objective of this work.

2. Experimental

Three types of experiments were carried out: (a) experiments to determine the influence of column diameter on the rise velocity of single spherical cap bubbles, (b) experiments to study in-line and off-line interactions of bubble pairs and (c) large bubble swarm velocity measurements in columns operating in the churn-turbulent regime.

2.1. Rise velocity of single spherical cap bubbles

The experiments were carried out in four cylindrical columns with different inside diameters: 0.051, 0.1, 0.174 and 0.63 m. The 0.051 m diameter column was made of glass while the other three columns were made of polyacrylate sections. Fig. 2 shows typical experimental setups. In all the experiments the top of the column was operated at atmospheric pressure. Demineralized water (viscosity $\mu_L = 0.001$ Pa s; density $\rho_L = 998$ kg/m^3; surface tension $\sigma = 0.072$ N/m) and Tellus oil ($\mu_L = 0.075$; $\rho_L = 862$; $\sigma = 0.028$) were used as liquid phase and air as gaseous phase. The experimental conditions are specified in Table 1.

For each experiment one single air bubble was injected at the bottom of the column using a standard medical syringe (syringes of different capacities were used in order to cover a wide range of bubble diameters). The 0.1, 0.174 and 0.63 m diameter columns were equipped with a ladle, which was mounted above the injection system, to allow bigger and more accurate gas volumes. To obtain the desired bubble volume the air was added into the ladle, by injecting air repeatedly with the small syringe. The bubble was released by inverting the ladle. The time elapsed for the single bubble to rise between predetermined markers was measured using a stopwatch. The distance between the two markers differed from column to column. In order to see the bubble passing the upper marker, a Sony colour video monitor was used. The Panasonic DSP colour CCD camera was focussed on the upper marker. The ambient light level was improved using a 1250 W halogen lamp. Corrections were applied for the bubble volume change due to the hydrostatic head differences during bubble rise and the average bubble diameter was determined on the basis of the

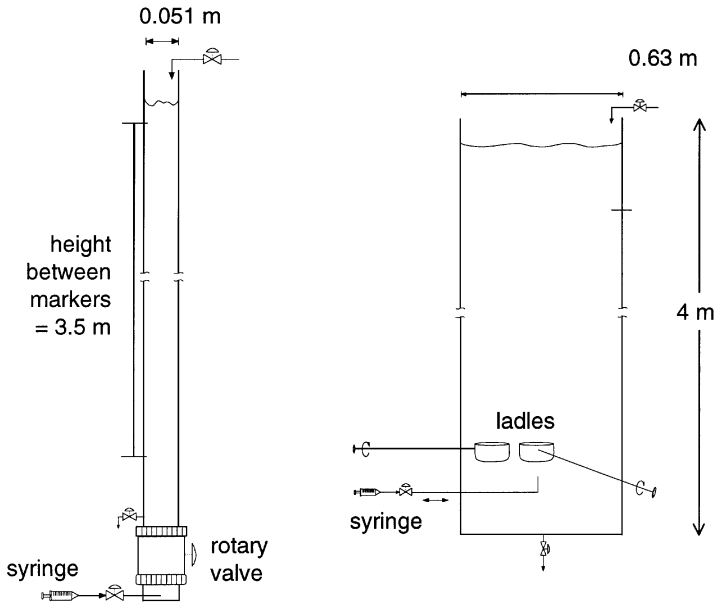

Fig. 2. Typical experimental set-ups for studies on rise velocity of single bubbles and bubble pairs.

Table 1
Experimental set-up details and operating conditions for gas–liquid single bubble experiments. Liquid phase properties are: demineralized water (viscosity $\mu_L = 0.001$ Pa s; density $\rho_L = 998$ kg/m^3; surface tension $\sigma = 0.072$ N/m) and Tellus oil ($\mu_L = 0.075$; $\rho_L = 862$; $\sigma = 0.028$)

Column diameter/(m)	Total height/(m)	Distance between markers/(m)	System studied	Injection system	Bubble diameter range/(mm)	Number of experiments
0.051	4	3.5	Air–water	Syringe	18–49	288
0.100	6	5	Air–water	Ladle	17–49	96
0.174	4	3.15	Air–water	Ladle	15–47	322
0.630	4	2.84	Air–water	Ladle	18–79	237
0.10	2	1	Air–Tellus oil	Syringe	13–72	147
Total number of experiments						1090

bubble volume calculated at the half-way position between the vertical markers.

2.2. In-line and off-line interactions of bubble pairs

In the 0.051 and 0.1 m diameter columns, bubbles of pre-determined volumes were injected in quick succession and their rise monitored and recorded on video at 25 frames/s for subsequent frame-by-frame analysis. In this manner in-line interactions of bubble pairs, of various size combinations could be studied. In-line interactions of air bubbles in water, Tellus oil, 86 wt% and 88 wt% glycerol solution were studied in the two columns. The 0.63 m diameter was equipped with two ladles (see Fig. 1), allowing off-line interactions of bubble pairs to be studied. In this case each of the two ladles were filled with pre-determined gas volumes and the ladles reversed to release these bubbles at either the same instant or with a pre-set time delay. The bubble trajectories were recorded on video tape at 25 frames/s using the image capturing set-up described in an earlier study (De Swart et al., 1996). Accurate determination of the bubble rise trajectories was obtained by analysis of the captured video images. The bubble contours of the captured video images were retraced manually using Micrografx designer version 4; these retraced images are reported later in this work. Though there is distortion of the bubble shapes due to the cylindrical columns used, the quantitative analysis of the bubble rise velocities and bubble accelerations are not affected because only the information with respect to the position of the bubble nose are used.

2.3. Measurement of large bubble swarm velocities in the churn-turbulent regime

In earlier work (Krishna and Ellenberger, 1996; De Swart, 1996) we had measured the large bubble swarm velocity in columns of 0.051, 0.1, 0.174, 0.19, 0.38 and 0.63 m in diameter with a variety of liquids using the dynamic gas disengagement technique (Schumpe and Grund, 1986). From this data bank we selected a data set measured with relatively low-viscosity liquids: water ($\rho_L = 998$; $\mu_L = 0.001$; $\sigma = 0.072$), tetradecane ($\rho_L = 763$; $\mu_L = 0.0022$; $\sigma = 0.027$), paraffin oil—A ($\rho_L = 795$; $\mu_L = 0.0023$; $\sigma = 0.028$) and paraffin oil—B ($\rho_L = 795$; $\mu_L = 0.0029$; $\sigma = 0.028$) for re-analysis to develop fundamentally based correlation for both sizes and rise velocity of the large bubbles. Additional large bubble swarm velocity data were obtained in this study with the system air–Tellus oil in columns of 0.1, 0.19 and 0.38 m diameter; see Table 2 for experimental conditions.

3. Rise velocity of single spherical cap bubbles

All of the 1090 experimental data points obtained in cylindrical columns met with the criterion $E\ddot{o} > 40$ (see Clift et al., 1978), ensuring that the bubbles were spherical cap in shape. In order to describe the rise velocity of these bubbles we introduce a scale factor correction into the Davies–Taylor (1950) relation

$$V_b^0 = 0.71\sqrt{gd_b}\,(\mathrm{SF}) \tag{3}$$

where the superscript 0 is used to emphasize that the rise velocity refers to that of a single, isolated, bubble. Collins (1967) has derived the following empirical relations for the scale factor:

$$\mathrm{SF} = 1 \quad \text{for } \frac{d_b}{D_T} < 0.125$$

$$\mathrm{SF} = 1.13\exp\left(-\frac{d_b}{D_T}\right) \quad \text{for } 0.125 < \frac{d_b}{D_T} < 0.6 \tag{4}$$

$$\mathrm{SF} = 0.496\sqrt{D_T/d_b} \quad \text{for } \frac{d_b}{D_T} > 0.6\,.$$

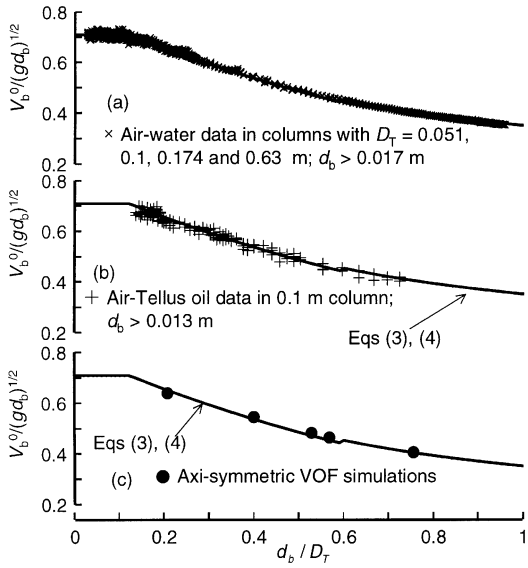

Fig. 3. Scale effects for rise of single gas bubbles in cylindrical columns. (a) comparison of data for air–water with the Davies–Taylor–Collins model, Eqs. (3) and (4). (b) comparison of data for air–Tellus oil with Eqs. (3) and (4). (c) Comparison of VOF simulations with Eqs. (3) and (4).

The measured experimental data conform exceedingly well with the calculations using Eqs. (3) and (4); see Fig. 3a and b for water and Tellus oil, respectively. The strong influence of scale on the bubble rise velocity is demonstrated graphically in Fig. 4 which shows retraced video images recording the rise of a 34 mm bubble in columns of 0.051 and 0.1 m diameter filled with water. It is to be noted that the bubble appears to be flatter in the 0.1 m diameter column.

4. Volume-of-fluid-simulations

To understand the scale effects on rise of spherical cap bubbles we undertook Volume-of-Fluid (VOF) simulations. The VOF model (Delnoij et al., 1997b; Hirt and Nichols, 1981; Tomiyama et al., 1993a,b) resolves the transient motion of the gas and liquid phases using the

Table 2
Experimental set-up details and operating conditions for holdup experiments with Tellus oil

Column diameter/(m)	Total height/(m)	System studied	Superficial gas velocity/(m/s)	Number of experiments
0.10	2	Air–Tellus oil	0.0002–0.2	67
0.19	4	Air–Tellus oil	0.0006–0.5	76
0.38	4	Air–Tellus oil	0.0007–0.5	57
Total number of experiments				200

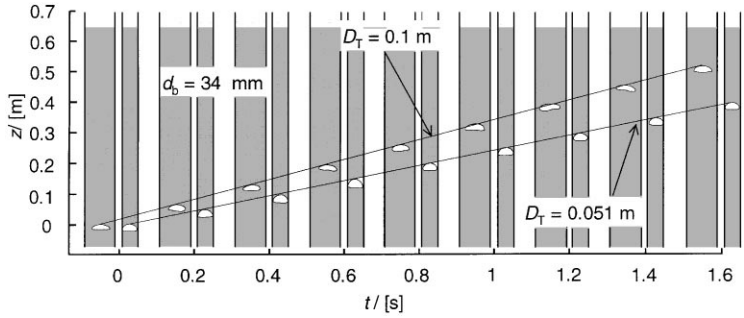

Fig. 4. Comparison of the rise trajectories of a 34 mm diameter bubble rising in water in columns of 0.051 and 0.1 m diameter. Experimentally obtained video images have been retraced.

Navier–Stokes equations, and accounts for the topology changes of the gas–liquid interface induced by the relative motion between the dispersed gas bubble and the surrounding liquid. The finite-difference VOF model uses a donor–acceptor algorithm, originally developed by Hirt and Nichols (1981), to obtain, and maintain, an accurate and sharp representation of the gas–liquid interface. The VOF method defines a fractional volume or 'colour' function $c(\mathbf{x}, t)$ that indicates the fraction of the computational cell filled with liquid. The colour function varies between 0, if the cell is completely occupied by gas, and 1, if the cell consists only of the liquid phase. The location of the bubble interface is tracked in time by solving a balance equation for this function:

$$\frac{\partial c(\mathbf{x}, t)}{\partial t} + \nabla\cdot(\mathbf{u}c(x, t)) = 0\,. \tag{5}$$

The liquid and gas velocities are assumed to equilibrate over a very small distance and essentially $\mathbf{u}_k = \mathbf{u}$ for $k = L,\ G$ at the bubble interface. The mass and momentum conservation equations can be considered to be homogenous

$$\nabla\cdot(\rho\mathbf{u}) = 0 \tag{6}$$

$$\frac{\partial \rho\mathbf{u}}{\partial t} + \nabla\cdot(\rho\mathbf{u}\mathbf{u}) = -\nabla p - \nabla\cdot\tau + \rho\mathbf{g} + \mathbf{F}_{sf} \tag{7}$$

where p is the pressure, τ is the viscous stress tensor, $\mathbf{g}$ is the gravitational force. The density and viscosity used in Eqs. (6) and (7) are calculated from

$$\rho = \varepsilon_L\rho_L + \varepsilon_G\rho_G, \quad \mu = \varepsilon_L\mu_L + \varepsilon_G\mu_G \tag{8}$$

where ε_k denotes the volume fraction of the phase $k = L,G$. The continuum surface force model, originally proposed by Brackbill et al. (1992), is used to model the force due to surface tension acting on the gas–liquid interface. In this model the surface tension is modelled as a body force $\mathbf{F}_{sf}$, that is non-zero only at the bubble interface and is given by the gradient of the colour function

$$\mathbf{F}_{sf} = \sigma\kappa(\mathbf{x})\nabla c(\mathbf{x}, t) \tag{9}$$

where $\kappa(\mathbf{x})$ is the local mean curvature of the bubble interface

$$\kappa(\mathbf{x}, t) = -\nabla\cdot\left(\frac{\mathbf{n}}{|\mathbf{n}|}\right) \tag{10}$$

where $\mathbf{n}$ is the vector normal to the bubble interface

$$\mathbf{n} = \nabla c(\mathbf{x}, t)\,. \tag{11}$$

The set of Eqs. (5)–(11) were solved using the commercial flow solver CFX 4.1c of AEA Technology, Harwell, UK. This package is a finite volume solver, using body-fitted grids. The grids are non-staggered and all variables are evaluated at the cell centers. An improved version of the Rhie-Chow (1983) algorithm is used to calculate the velocity at the cell faces. The pressure–velocity coupling is obtained using the SIMPLEC algorithm (Van Doormal and Raithby, 1984).

Table 3 lists the VOF simulations performed for single bubbles rising in a cylindrical column filled with liquid, which was taken to be either water, paraffin oil or ethylene glycol. Since spherical cap bubbles rise vertically in a straight line, axi-symmetry was assumed in these simulations. A uniform grid of 1 mm size in both r- and z-directions was used. The column was modeled as an open system, so the pressure in the gas space above the initial liquid column is equal to the ambient pressure (101.325 kPa). For the convective terms in the equations hybrid differencing was used. Upwind differencing was used for the time integration. The time step used in the simulations were usually 0.0004 s or smaller. To counteract excessive smearing of the liquid–gas interface by numerical diffusion, a surface sharpening routine was invoked. This routine identifies gas and liquid on the 'wrong' side of the interface, and moves it back to the correct side, while conserving volume of the respective phases. In order to avoid 'dissolution' of the bubble due to surface sharpening we found it necessary to ensure that each bubble area encompassed a few hundred cells; a grid cell size of 1 mm satisfied this requirement and in all the simulations there was less than 10% volume

Table 3
Results of axi-symmetric VOF simulations in cylindrical coordinates. In all cases the grid size chosen was Δr, $\Delta z = 1$ mm.The systems were either air–water (see properties in Table 2), Air–paraffin oil ($\rho_L = 795$; $\mu_L = 0.0023$; $\sigma = 0.028$) or air–ethylene glycol ($\rho_L = 1109$; $\mu_L = 0.0199$; $\sigma = 0.0477$)

Bubble diameter, d_b/(m)	Column diameter, D_T/(m)	System	Time step, Δt/(s)	Rise velocity, V_b/(m s^1)
0.021	0.1	Air–water	0.0004	0.289
0.021	0.051	Air–water	0.0004	0.244
0.029	0.051	Air–water	0.0004	0.248
0.027	0.051	Air–paraffin oil	0.0003	0.249
0.039	0.051	Air–ethylene glycol	0.0003	0.25

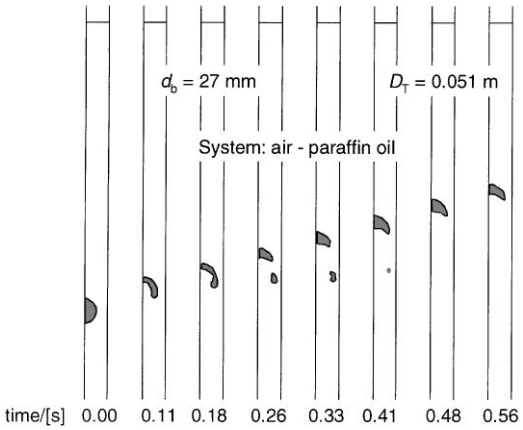

Fig. 5. Snapshots obtained with axi-symmetric cylindrical VOF simulations of rise of a 27 mm diameter bubble in a column of 0.051 m diameter. The system is air – paraffin oil.

(or area) change during the simulation. Simulations carried out with a 2 mm grid size did not meet with the above requirement while simulations with a finer grid size than 1 mm did not yield significantly different results.

All simulations were carried out using the parallel version of CFX 4.1c running on Silicon Graphics Power Challenge machine with six R8000 processors. To give an indication of the required CPU time, the axi-symmetric simulation of the rise of a 27 mm bubble for 0.83 s in a 0.051 m diameter cylindrical column of 0.5 m height, filled with paraffin oil, involving 13,000 grid cells took 4 days. Snapshots at various time steps for this simulation are shown in Fig. 5. As initial condition a spherical bubble, was placed near the bottom of the column. To ensure convergence in the initial period when the bubble 'adjusts' itself to its surrounding and begins its ascent, the following time stepping strategy was used: 50 steps at 5×10^{-5} s, 50 steps at 2.5×10^{-5} s, 50 steps at 5×10^{-5} s and 3000 steps at 3×10^{-4} s. For each time step about 40 iterations were typically required to obtain convergence of the governing equations. The grid size and time steps used in our work are significantly finer than those used by other workers using VOF simulations (e.g. Delnoij et al., 1997a). This would tend to compensate for the fact that the Hirt–Nichols Donor–Acceptor algorithm used in the CFX implementation of the VOF algorithm is considered to be rather 'crude' compared to the more sophisticated algorithms available currently (Delnoij et al., 1997a). It can be noted from Fig. 5 that small fragments of the bubble are torn off in the initial stages and these fragments 'dissolve' away due to application of the surface sharpening procedure and also due to numerical diffusion. The bubble diameters reported in Table 3 were determined from the volume of the remaining bubble, which typically attains its terminal velocity after about 0.15 s from the start of the simulation. The bubble rise velocity was determined by a linear regression of the z-coordinates of the nose of the bubble during steady-rise.

Fig. 6 compares the z-coordinates of the nose of 21 mm bubbles rising in columns of 0.1 and 0.051 m diameters filled with water; this figure shows that the bubble rises faster in the wider column. The reason for this is the restraining effect of the walls. The insets to Fig. 6 show the liquid phase velocity profiles for these two simulations. We notice that the 21 mm bubble assumes a flatter shape in the 0.1 m wide column and is less influenced by the wall than the same bubble placed in a 0.051 m wide column. This is in accordance with the video images obtained experimentally; see Fig. 4. Put another way, the drag between the bubble and the liquid is higher in the column of smaller width due to the higher downward liquid velocity in the vicinity of the bubble.

The five axi-symmetric cylindrical simulations for air–water, air–paraffin oil and air–ethylene glycol are in excellent agreement with the Davies–Taylor–Collins relations (3, 4); see Fig. 3c. Since the simulations were

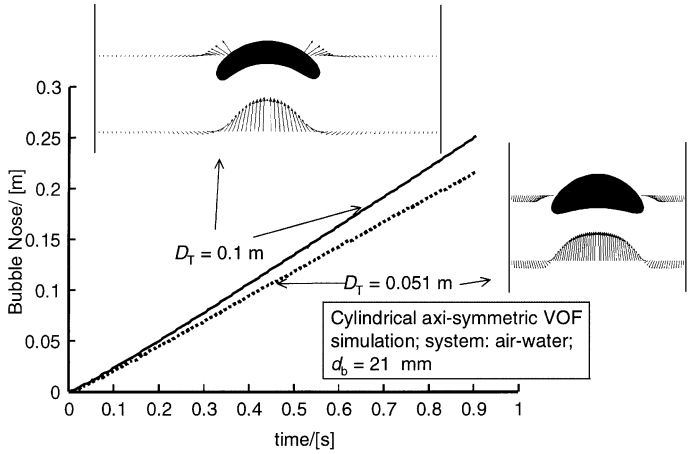

Fig. 6. VOF simulations of the rise trajectories of a 21 mm diameter bubble in 0.051 and 0.1 m diameter columns. The insets show the liquid phase velocity profiles surrounding the bubble.

carried out with widely varying density, surface tension and viscosity values, we also conclude the general validity of Eqs. (3) and (4) provided the condition of $Eö > 40$ is met.

5. Off-line and in-line interactions of bubble pairs

Our earlier work on video image analysis of large bubble swarms (De Swart et al., 1996) showed a wide distribution of bubble sizes, ranging from 20 to 80 mm. The bubbles in the swarm were observed to be constantly coalescing and breaking up. The coalescence and breakup frequencies ranged from 2 to 20 s^{-1}, increasing with increasing bubble sizes. Before building up an understanding of the bubble swarms, let us consider the interactions between bubble pairs. In-line interactions of bubble pairs have been the subject of earlier studies (Bhaga and Weber, 1980; Komasawa et al., 1980; Narayanan et al., 1974); here we shall attempt to quantify these interactions for use later in developing a model for the large bubble swarm velocity.

Fig. 7 shows the retraced pictures of video recordings of the rise of two 47 mm diameter bubbles in the 0.63 m diameter column when their starting vertical positions are at the same horizontal plane. The horizontal distance of separation of these two bubbles is 0.12 m. The two bubbles rise at the same velocity, corresponding to the value they would have were they to be injected individually. Their rise velocities are not affected by each other. However, when the starting vertical positions of these two 47 mm bubbles are slightly different (0.07 m vertical separation), the trailing bubble quickly gets sucked into the wake of the leading bubble and during this process it experiences an accelerated rise; see Fig. 8. Note that the trailing bubble gets vertically aligned with the leading bubble before coalescence occurs.

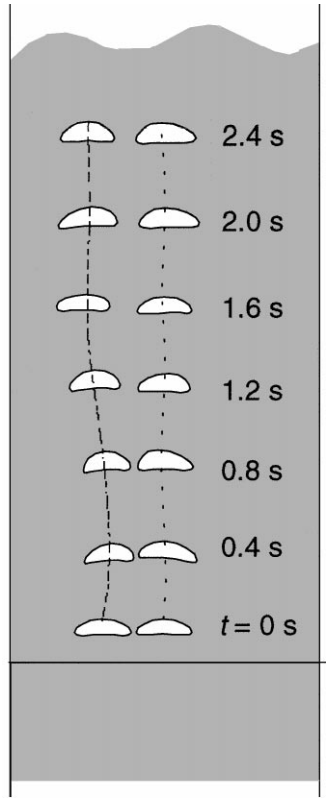

Fig. 7. Rise trajectories of two 47 mm diameter bubbles in water, separated by a horizontal distance of 0.12 m. Both bubbles are released simultaneously. Column diameter is 0.63 m.

Fig. 9 shows another experiment in which the initial position of two bubbles, of 40 and 50 mm sizes are horizontally aligned. As expected, the 50 mm bubble rises faster and accelerates the smaller bubble until coalescence takes place. Note again that the smaller 40 mm trailing bubble aligns itself vertically behind the leading bubble before coalescence occurs.

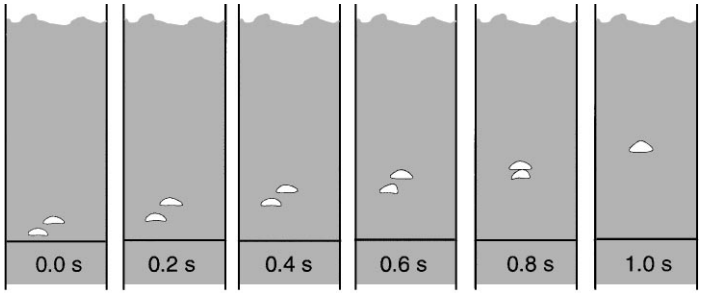

Fig. 8. Rise trajectories of two 47 mm diameter bubbles in water, separated by 0.1 m horizontally. Initial vertical separation is 0.07 m between the two bubbles. Column diameter is 0.63 m.

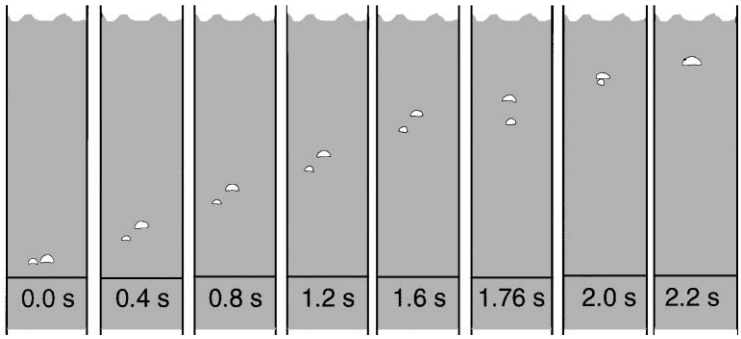

Fig. 9. Rise trajectories of two bubbles in water, 40 and 50 mm in diameter, separated by 0.1 m horizontally. Both bubbles are released simultaneously. Column diameter is 0.63 m.

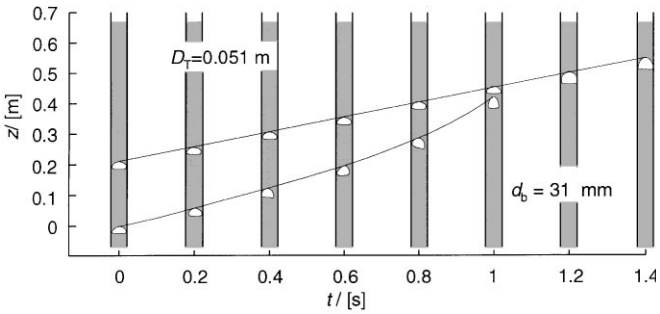

Fig. 10. Retraced video images of in-line interactions of 31 mm diameter bubbles rising in a 0.051 m diameter column filled with water.

In order to quantify the acceleration effect experienced by the trailing bubble, we studied vertical in-line interactions of pairs of bubbles of differing sizes in the 0.051 and 0.1 m diameter columns filled with water, aqueous glycerol solutions or Tellus oil. Typical rise trajectories are shown in Fig. 10 for the in-line interactions of two 31 mm diameter bubbles in water. It is clear that the acceleration effect increases as the trailing bubble approaches the leading bubble. The VOF simulation of this experiment is shown in Fig. 11. The reason that the shape of the bubbles in the VOF simulations appears to be hollower than in the experiment is due to the fact that in the video recordings only the outer periphery of the bubbles can be visualized. The contours of the bubbles in Fig. 11, however, are drawn for a slice in the r–z plane. The liquid phase velocity profiles at 0.07 s before coalescence of the bubbles are indicated in the inset in Fig. 11. The trailing bubble gets sucked into the wake of the leading bubble. A comparison of the measured trajectories for both leading and trailing bubbles with VOF simulations shows very good agreement; see Fig. 12. A similar good agreement between VOF simulations and experiment is obtained for the rise trajectories of two 31 mm bubbles rising in aqueous 86 wt% glycerol solution with a viscosity of 0.1 Pa s; see Fig. 12. Animations of the VOF simulations performed to study in-line interactions of bubbles in various liquids can be viewed on our web site (*http://ct-cr4.chem.uva.nl/axissym*).

The slope of the rise trajectory at any instant of time yields the rise velocity. We define an acceleration factor, AF, for the trailing bubbles as the ratio of the actual velocity to the velocity it would have were the same bubbles uninfluenced by other bubbles; this latter velocity can be obtained from Eqs. (3) and (4). In Fig. 13, the experimentally observed acceleration factor for the

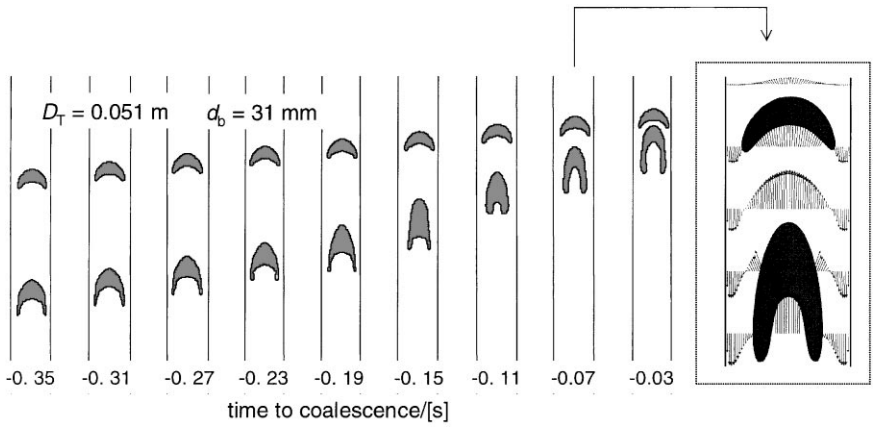

Fig. 11. VOF simulations, using cylindrical axi-symmetry, of the experiment shown in Fig. 10. The inset shows the liquid phase velocity profiles for the situation corresponding to 0.07 s before coalescence. Animations of this VOF simulation can be viewed on our web site (*http://ct-cr4.chem.uva.nl/axissym*).

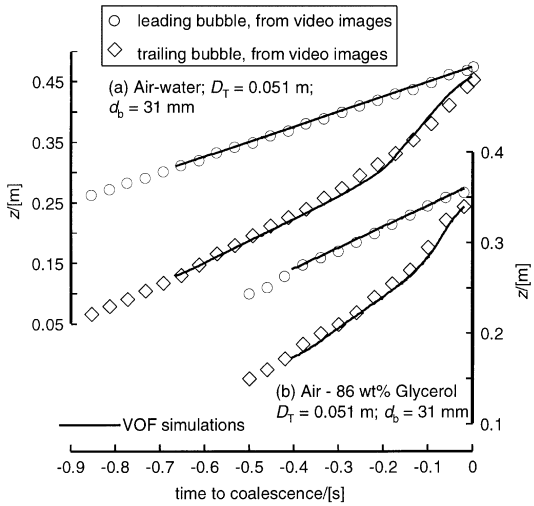

Fig. 12. Comparison between experiment and VOF simulations of the rise trajectories of the leading and trailing bubbles in a 0.051 m diameter column filled with (a) water and (b) 86 wt% glycerol solution. Animations of these VOF simulations can be viewed on our web site (*http://ct-cr4.chem.uva.nl/axissym*).

trailing bubble is plotted against its distance of separation, Δz, from the leading bubble. The acceleration factor AF is seen to increase as Δz decreases in a more or less linear fashion. For a given separation distance, the value of AF decreases with increasing liquid viscosity. For example when $\Delta z = 0.05$ m, the value of AF for water ($\mu_L = 0.001$) is 3, for Tellus oil ($\mu_L = 0.075$), AF = 2.5 and for 86 wt% glycerol ($\mu_L = 0.147$), AF = 2. The wake interaction effects are weaker in highly viscous liquids. The wake interaction effects in low-viscosity liquids (say with $\mu_L < 0.003$ Pa s) can be expected to be of comparable magnitude.

6. Rise velocity of large bubble swarms

For steady-state mode of operation in the churn-turbulent regime (see Fig. 1), every large bubble is a 'trailing' bubble. The large bubble swarm velocity can therefore be expected to be much higher than that of a single, isolated, bubble, V_b^0. From the foregoing section we should expect the acceleration factor to increase linearly with decreasing distance of separation of the bubbles. With increasing values of $(U - U_{\text{trans}})$ we should expect the average distance of separation between the large bubbles to decrease. We therefore assert that

$$V_b = V_b^0(\text{AF}); \quad \text{AF} = \alpha + \beta(U - U_{\text{trans}}) \tag{12}$$

where V_b^0 is given by eqs (3) and (4). The experimental data on V_b as a function of $(U - U_{\text{trans}})$ we collected earlier (Krishna and Ellenberger, 1996; De Swart, 1996), comprising more than 1000 measured points with liquids of relatively low viscosity (less than 0.0029 Pa s) were used to obtain the following expressions for the average large bubble diameter and the acceleration factor, AF:

$$\begin{aligned} d_b &= 0.069(U - U_{\text{trans}})^{0.376}, \\ \text{AF} &= 2.73 + 4.505(U - U_{\text{trans}}) \end{aligned} \tag{13}$$

In obtaining the fits, only experimental data with $(U - U_{\text{trans}})$ values exceeding 0.05 m/s were used. This truncation was necessary in order to ensure that the large bubble sizes met with the $E\ddot{o} > 40$ criterion required of the Davies–Taylor–Collins relations (3) and (4). The four fit parameters in Eq. (13) were determined by the multiple regression solver routine of Microsoft Excel 97 in which the mean-square deviation between experiments and model equations were minimized. The correlation (13) is only valid when the $E\ddot{o} > 40$ criterion is met for the

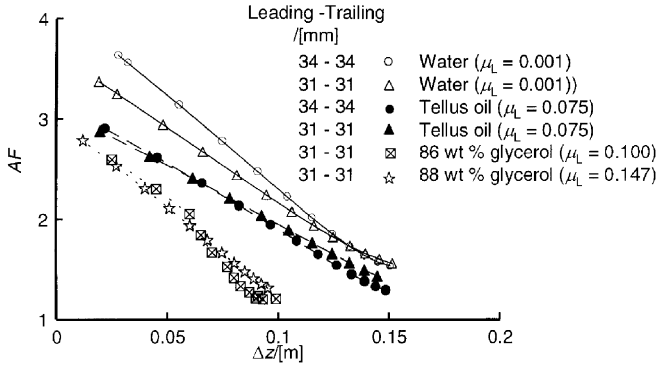

Fig. 13. The acceleration factor for the trailing bubble as function of its distance of separation from the preceding bubble. The measurements with Tellus oil were made in a 0.1 m diameter column and those with water and 86 wt% aqueous glycerol solution were made in a 0.051 m diameter column.

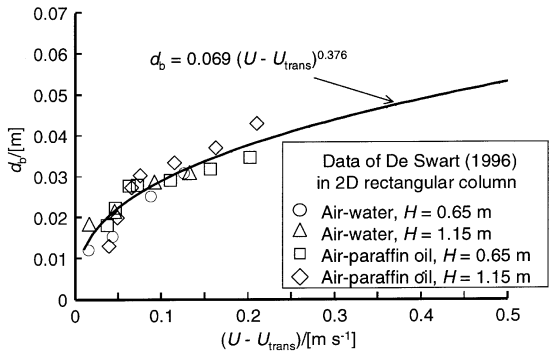

Fig. 14. Correlation for the average bubble size of large bubble swarm as function of the superficial gas velocity through the large bubble population. The experimental data is from De Swart (1996) measured with the systems air–water and air–paraffin oil in a 2D rectangular column of 0.3 m width at different heights H above the distributor.

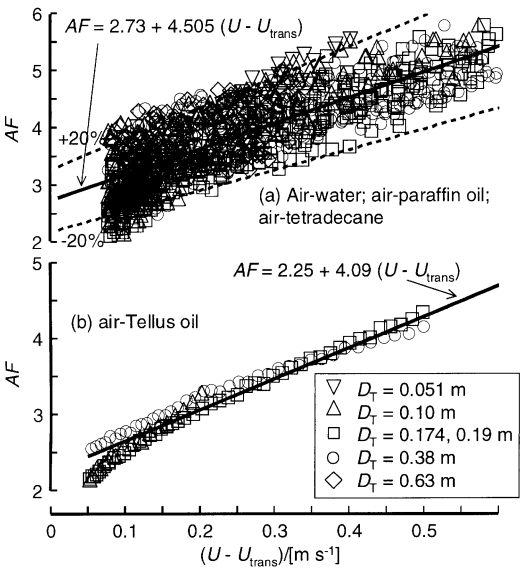

Fig. 15. The acceleration factor for large bubble velocity swarm in (a) low-viscosity liquids (water, paraffin oil, tetradecane) and (b) high-viscosity liquids (Tellus oil).

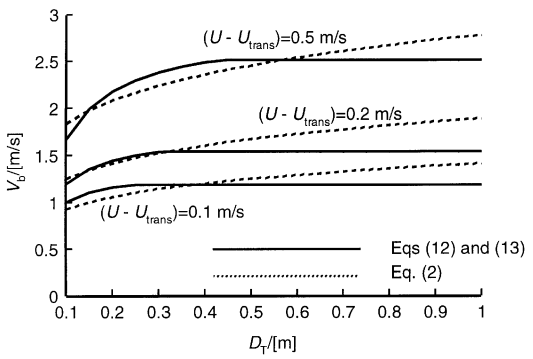

Fig. 16. Comparison of the predictions of the large bubble swarm velocity due to Krishna and Ellenberger (1996) and that developed in this paper, Eqs. (12) and (13).

predicted bubble sizes. The fitted bubble size correlation agrees remarkably well with the measured data on average large bubble diameters carried out earlier in our group (De Swart, 1996; De Swart et al., 1996) for the systems air–water and air– paraffin oil in a 2D rectangular column of 0.3 m width; see Fig. 14. There are no other reported large bubble size correlations available in the literature. In Fig. 15a we compare the experimental values of the acceleration factor AF (calculated with the fitted bubble size expression) against the correlation line. There is about a 20% spread in the experimental data around the correlation line; cf. Fig. 15a. A detailed examination of the experiments reported in Fig. 15a has shown that there is no systematic deviation of the measured data obtained in columns of various diameters from the developed correlation for AF, Eq. (13). This evidence supports our assertion that the scale correction factor, SF, is correctly represented and the same as for a single isolated spherical cap bubble [see Eq. (4)].

The predictions of Eqs. (12) and (13) for various column diameters and $(U - U_{trans}) = 0.1$, 0.2 and 0.5 m/s are compared in Fig. 16 with those of the Krishna–Ellenberger 1996) Eq. (2). It is to be noted that for column diameters below 0.5 m, the predictions of the method developed in this paper agree quite well with our earlier correlation. This is not surprising considering that the same data set has been used to develop our new, more fundamental approach. The important differences arise when extrapolating to column diameters exceeding 0.5 m. The current approach predicts that the rise velocity reaches a plateau value for column diameters exceeding about 0.5 m, an intuitively acceptable result. The power-law correlation (2), however, predicts a steady increase of V_b for column diameters exceeding 0.5 m; this increase cannot be expected to proceed indefinitely.

In order to demonstrate the validity of our estimation procedure for V_b we shall attempt to predict the total gas holdup for an air–water bubble column of 0.2 m diameter. Experimental measurements on such a column have been reported by Hyndman et al. (1997). They determined the values of the transition parameters as: $U_{\text{trans}} = 0.0375$ m/s, $\varepsilon_{\text{trans}} = 0.137$. The total gas holdup in the churn-turbulent regime, prevailing for $U > U_{\text{trans}}$ is calculated from the model suggested by Krishna and Ellenberger (1996)

$$\varepsilon = \varepsilon_b + \varepsilon_{\text{trans}}[1 - (U - U_{\text{trans}})/V_b];$$
$$\varepsilon_b = (U - U_{\text{trans}})/V_b. \tag{14}$$

The calculations for ε using Eqs. (12)–(14) for V_b are in remarkably good agreement with the experimental data of Hyndman et al. (1997); see Fig. 17.

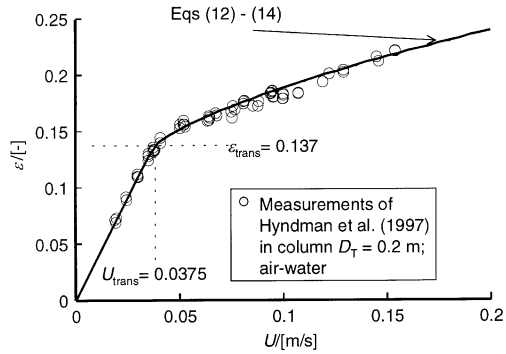

Fig. 17. Comparison of the predictions of the total gas holdup using the Eqs. (12), (13) and (14) with the experimental data of Hyndman et al. (1997).

From the new measurements we made in this study with the system air – Tellus oil ($\mu_L = 0.075$), the corresponding fits for the bubble size and acceleration factors are

$$d_b = 0.076(U - U_{\text{trans}})^{0.438},$$
$$\text{AF} = 2.31 + 3.82(U - U_{\text{trans}}). \tag{15a}$$

This fitted bubble size relation yields values so remarkably close to that for low viscous liquids, Eq. (13), that we refitted the experimental data choosing a common bubble size relationship for both low- and high-viscous liquids; the refitted relations which we recommend for Tellus oil are

$$d_b = 0.069(U - U_{\text{trans}})^{0.376},$$
$$\text{AF} = 2.25 + 4.09(U - U_{\text{trans}}). \tag{15b}$$

As expected the AF for the high-viscosity Tellus oil is lower by about 20% than for low-viscosity liquids such as water and paraffin oil; see Fig. 15b. Comparison of the experimental data for the large bubble holdup for 0.1, 0.19 and 0.38 m diameter columns with calculations using Eqs. (12), (14) and (15b) confirms the accuracy of our fits and calculation procedure. The significant influence of the column diameter on the large bubble holdup is evident, emphasizing the importance of taking scale effects into account when estimating the large bubble swarm velocity.

The results of the present paper can be easily incorporated into CFD models of bubble columns by using the drag coefficient defined by

$$C_D = \frac{4}{3}\frac{\rho_L - \rho_G}{\rho_L} g d_b \frac{1}{V_b^2} \tag{16}$$

for the large bubble population. The drag coefficient thus calculated represents an averaged value over the range of bubble sizes actually encountered in practice. The acid

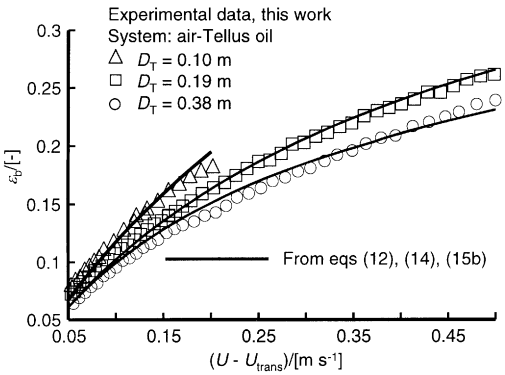

Fig. 18. Comparison of the predictions of the large bubble holdup using the Eqs. (12), (14) and (15b) with the experimental data generated in this work for the system air–Tellus oil (Table 2).

test of the validity of the developed drag relation would be to carry out Eulerian simulations of bubble columns in the churn-turbulent regime. In a companion study, incorporating a three-phase Eulerian simulation of bubble columns of 0.14, 0.174, 0.38 and 0.63 m diameter, we have demonstrated the validity of these drag relations (Krishna and van Baten, 1998) by comparison with experimental data.

7. Conclusions

1. For rise of single spherical cap bubbles (meeting with the criterion $Eö > 40$) in cylindrical columns, the Davies–Taylor–Collins relations (3) and (4) are found to be of excellent accuracy. VOF simulations, using axi-symmetric cylindrical coordinate geometry, are in excellent agreement with experiments and represent a powerful tool for *a priori* prediction of scale effects on single bubble rise for gas–liquid systems with widely varying properties.

2. Experimental studies of in-line interaction between bubble pairs showed that the trailing bubble rise velocity is enhanced as the distance of separation is decreased. VOF simulations allow *a priori* calculation of the rise trajectories of leading and trailing bubbles.
3. The acceleration factor AF depends on the liquid viscosity; higher viscosities lead to lower wake acceleration effects.
4. For the rise of large bubble swarms in bubble columns operating in the churn-turbulent regime, the scale factor is the same as that given by the Collins relation (4).
5. The empirically fitted relations (13) and (15) allow estimation of the large bubble size and acceleration factor in liquids of low- and high-viscosity, respectively.

Notation

AF	acceleration factor, dimensionless
$c(\mathbf{x}, t)$	colour function, dimensionless
C_D	drag coefficient, dimensionless
d_b	equivalent bubble diameter, m
D_T	cylindrical column diameter, m
$Eö$	Eötvös number, $g\mu_L(\rho_L - \rho_G)d_b^2/\sigma$
$\mathbf{F}_{sf}$	surface tension force, N/m^3
g	acceleration due to gravity, 9.81 m/s^2
H	height above distributor, m
$\mathbf{n}$	vector normal to the interface
r	radial coordinate, m
SF	scale correction factor, dimensionless
t	time, s
$\mathbf{u}$	velocity vector, m/s
U	superficial gas velocity, m/s
$(U - U_{\text{trans}})$	superficial gas velocity through the large bubble phase, m/s
U_{trans}	superficial gas velocity at the regime transition point, m/s
V_b	rise velocity of the bubble, m/s
x	x-coordinate in cartesian geometry
z	distance coordinate along height of cylindrical column, m
Δz	distance between leading and trailing bubbles, m

Greek letters

α,β	parameters defined by Eq. (12)
ε	volume fraction of phase, dimensionless
$\varepsilon_{\text{trans}}$	gas holdup at the regime transition point, dimensionless
$\kappa(\mathbf{x})$	curvature of bubble interface, dimensionless
μ	viscosity of phase, Pa s
ρ	density of phases, kg/m^3
σ	surface tension of liquid phase, N/m
τ	viscous stress tensor, N/m^2

Subscripts

b	referring to large bubble population
G	referring to gas phase
L	referring to liquid phase
trans	regime transition point
T	tower or column

Superscript

0	referring to single isolated bubble

References

Bhaga, D., & Weber, M.E. (1980). In-line interaction of a pair of bubbles in a viscous liquid. *Chem. Engng Sci., 35*, 2467–2474.

Boisson, N., & Malin, M.R. (1996). Numerical prediction of two-phase flow in bubble columns. *Int. J. Numeri. Meth. Fluids., 23*, 1289–1310.

Brackbill, J.U., Kothe, D.B., & Zemarch, C. (1992). A continuum method for modelling surface tension. *J. Comput. Phys., 100*, 335–354.

Clift, R., Grace, J.R., & Weber, M.E. (1978). *Bubbles, drops and particles.* San Diego, Academic Press.

Collins, R. (1967). The effect of a containing cylindrical boundary on the velocity of a large gas bubble in a liquid. *J. Fluid Mech., 28*, 97–112.

Davies, R.M., & Taylor, G.I. (1950). The mechanics of large bubbles rising through extended liquids and through liquids in tubes. *Proc. Roy. Soc. London., A200*, 375–390.

Delnoij, E., Kuipers, J.A.M., & van Swaaij, W.P.M. (1997a). Computational fluid dynamics applied to gas–liquid contactors. *Chem. Engng. Sci., 52*, 3623–3638.

Delnoij, E., Lammers, F.A., Kuipers, J.A.M., & van Swaaij, W.P.M. (1997b). Dynamic simulation of dispersed gas–liquid two-phase flow using a discreet bubble model. *Chem. Engng. Sci., 52*, 1429–1458.

Devanathan, N., Dudukovic, M.P., Lapin, A., & Lübbert, A. (1995). Chaotic flow in bubble column reactors. *Chem. Engng. Sci., 50*, 2661–2667.

Van Doormal, J., & Raithby, G.D. (1984). Enhancement of the SIMPLE method for predicting incompressible flows. *Numer. Heat Transfer., 7*, 147–163.

Fan, L.S., & Tsuchiya, K. (1990). *Bubble Wake Dynamics in Liquids and Liquid–Solid Suspensions.* Boston: Butterworth–Heinemann.

Grevskott, S., Sannæs, B.H., Dudukovic, M.P., Hjarbo, K.W., & Svendsen, H.F. (1996). Liquid circulation, bubble size distributions, and solids movement in two- and three-phase bubble columns. *Chem. Engng. Sci., 51*, 1703–1713.

Grienberger, J., & Hofmann, H. (1992). Investigations and modelling of bubble columns. *Chem. Engng. Sci., 47*, 2215–2220.

Hirt, C.W., & Nichols, B.D. (1981). Volume of fluid (VOF) method for the dynamics of free boudaries. *J. Comput. Phys., 39*, 201–225.

Hyndman, C.L., Larachi, F., & Guy C. (1997). Understanding gas-phase hydrodynamics in bubble columns: a convective model based on kinetic theory. *Chem. Engng. Sci., 52*, 63–77.

Jakobsen, H.A. (1993). *On the modelling and simulation of bubble column reactors using a two-fluid model.* Dr. Ing. thesis. The University of Trondheim, The Norwegian Institute of Technology, Department of Chemical Engineering, Trondheim.

Jakobsen, H.A., Sannæs, B.H., Grevskott, S., & Svendsen, H.F. (1997). Modeling of bubble driven vertical flows. *Ind. Engng. Chem. Res., 36*, 4052–4074.

Komasawa, I., Otake, T., & Kamojima, M. (1980). Wake behaviour and its effect on interaction between spherical-cap bubbles. *J. Chem. Engng. Japan.*, *13*, 103–109.

Krishna, R., & Ellenberger, J. (1996). Gas holdup in bubble column reactors operating in the churn-turbulent flow regime. *A.I.Ch.E.J.*, *42*, 2637–2634.

Krishna, R., Ellenberger, J., & Sie, S.T. (1996). Reactor development for conversion of natural gas to liquid fuels: A scale up strategy relying on hydrodynamic analogies. *Chem. Engng. Sci.*, *51*, 2041–2050.

Krishna, R., & Van Baten, J.M. (1998). Three-phase Eulerian simulations of bubble column reactors operating in the churn-turbulent regime. *Chem. Engng. Sci.*, submitted.

Kumar, S., Vanderheyden, W.B., Devanathan, N., Padial, N.T., Dudukovic, M.P., & Kashiwa, B.A. (1995). Numerical simulation and experimental verification of gas–liquid flow in bubble columns. *Industrial Mixing Fundamentals with Applications*, *A.I.Ch.E. Symposium Series No.* 305, (Vol 91, pp. 11–19).

Lapin, A., & Lübbert, A. (1994). Numerical simulation of the dynamics of two-phase gas–liquid flows in bubble columns. *Chem. Engng. Sci.*, *49*, 3661–3674.

Lin, T.J., Reese, J., Hong, T., & Fan, L.S. (1996). Quantitative analysis and computation of two-dimensional bubble columns. *A.I.Ch.E.J.*, *42*, 301–318

Narayanan, S., Goossens, L.H.J., & Kossen, N.W.F. (1974). Coalescence of two bubbles rising in a line at low Reynolds numbers. *Chem. Engng. Sci.*, *29*, 2071–2082.

Ranade, V.V. (1992). Flow in bubble columns: some numerical experiments. *Chem. Engng. Sci.*, *47*, 1857–1869.

Reilly, I.G., Scott, D.S., De Bruijn, T.J.W., & MacIntyre, D. (1994). The role of gas phase momentum in determining gas holdup and hydrodynamic flow regimes in bubble column operations. *Can. J. Chem. Engng.*, *72*, 3–12.

Rhie, C.M., & Chow, W.L. (1983). Numerical study of the turbulent flow past an airfoil with trailing edge separation. *AIAA J.*, *21*, 1525–1532.

Schumpe, A., & Grund, G. (1986). The gas disengagement technique for studying gas holdup structure in bubble columns. *Can. J. Chem. Engng.*, *64*, 891–896.

Sokolichin, A., & Eigenberger, G. (1994). Gas–liquid flow in bubble columns and loop reactors: Part I. Detailed modelling and numerical simulation. *Chem. Engng. Sci.*, *49*, 5735–5746.

Sokolichin, A., Eigenberger, G., Lapin, A., & Lübbert, A. (1997). Direct numerical simulation of gas–liquid two-phase flows. Euler/Euler versus Euler/Lagrange. *Chem. Engng. Sci.*, *52*, 611–626.

De Swart, J.W.A. (1996). *Scale up of a Fischer Tropsch slurry reactor*, Ph.D. thesis in Chemical Engineering, University of Amsterdam, Amsterdam.

De Swart, J.W.A., Van Vliet, R.E., & Krishna, R. (1996). Size, structure and dynamics of 'large' bubbles in a 2-D slurry bubble column. *Chem. Engng. Sci.*, *51*, 4619–4629.

Tomiyama, A., Sou, A., Minagawa, H., & Sakaguchi, T. (1993a). Numerical analysis of a single bubble by VOF method. *JSME Int. J. Series B*, *36*, 51–56.

Tomiyama, A., Zun, I., Sou, A., & Sakaguchi, T. (1993b). Numerical analysis of bubble motion with the VOF method. *Nucl. Engng. Des.*, *141*, 69–82.

Torvik, R., & Svendsen, H.F. (1990). Modelling of slurry reactors. A fundamental approach. *Chem. Engng. Sci.*, *45*, 2325–2332.

Wezorke, H. (1986). *Einfluss von grossblasen in blasensäulenreaktoren*. Ph.D. dissertation. University of Dortmund, Germany.

Wilkinson, P.M., Spek, A.P., & Van Dierendonck, L.L. (1992). Design parameters estimation for scale-up of high-pressure bubble columns. *A.I.Ch.E.J.*, *38*, 544–554.